Exchange and crystal field effects on the $4f^{n-1}5d$ levels of Tb^{3+}

2003 J. Phys.: Condens. Matter 15 6249

(http://iopscience.iop.org/0953-8984/15/36/313)

INSTITUTE OF PHYSICS PUBLISHING JOURNAL OF PHYSICS: CONDENSED MATTER

J. Phys.: Condens. Matter **15** (2003) 6249–6268 PII: S0953-8984(03)64851-4

Exchange and crystal field effects on the $4f^{n-1}5d$ levels of Tb^{3+}

P Dorenbos

Interfaculty Reactor Institute, Delft University of Technology, Mekelweg 15, 2629 JB Delft, The Netherlands

E-mail: dorenbos@iri.tudelft.nl

Received 16 June 2003
Published 29 August 2003
Online at stacks.iop.org/JPhysCM/15/6249

Abstract

The levels of the $4f^{n-1}5d$ configuration of Ce^{3+} ($n = 1$), Pr^{3+} ($n = 2$), and Tb^{3+} ($n = 8$) in compounds are compared with each other. A model is presented that, by means of energy shift operations performed on the five 5d levels of Ce^{3+}, reproduces the energies of those for Pr^{3+} and Tb^{3+}. Using Tb^{3+} data, two main sources of deviations from the shift model are identified. One is related to the size difference between Tb^{3+} and Ce^{3+} which affects the lattice relaxation and the crystal field splitting of the 5d configuration. The other is related to the isotropic exchange interaction between the 5d electron spin and the total spin of the $4f^7$ electrons in Tb^{3+}. The exchange splitting is about 1 eV in fluorides, sulfates, and phosphates. In oxides with less strongly bonded oxygen 2p electrons, the exchange splitting decreases to 0.6 eV. The effects of the two deviations on the predictability of the $4f^{n-1}5d$ energy levels of Tb^{3+} and other lanthanides are discussed.

1. Introduction

Evidence is accumulating rapidly that on the basis of simple energy shift operations the location of $4f^{n-1}5d$ energy levels of a lanthanide ion in a compound can be predicted from that observed for Ce^{3+} in the same compound. This is particularly evident for the *first* $4f^{n-1}5d$ energy level. The energy $E(n, Q, \mathrm{A})$ needed for the transition from the $4f^n$ ground state to this level is given by [1]

$$E(n, Q, \mathrm{A}) = E_{\mathrm{Afree}}(n, Q) - D(Q, \mathrm{A}). \tag{1}$$

Here, a generalized notation is used. n is the number of electrons in the $4f^n5d^0$ configuration, $Q = 2+$ or $3+$ is the ionic charge of the lanthanide, and A stands for the name of the compound. $E_{\mathrm{Afree}}(n, Q)$ is for each lanthanide a constant. The values for E_{Afree} are close to the transition energy of the free ions. $D(n, Q, \mathrm{A})$ is the red-shift in the lanthanide with n electrons in the $4f^n$ configuration in compound A. It expresses the energy shift of the lowest $4f^{n-1}5d$ level due to

the interaction of the 5d electron with the crystalline environment. Within ±5%, $D(n, Q, \mathrm{A})$ appears the same for each lanthanide. One may then omit the variable n, and the red-shift $D(Q, \mathrm{A})$ becomes a property that characterizes a compound.

The red-shift for Ce^{3+} can be written as [2]

$$D(1, 3+, \mathrm{A}) = \epsilon_c(1, 3+, \mathrm{A}) + \frac{\epsilon_{cfs}(1, 3+, \mathrm{A})}{r(\mathrm{A})} - 0.234\ \mathrm{eV} \tag{2}$$

where $\epsilon_c(1, 3+, \mathrm{A})$ is defined as the shift of the barycentre energy of the 5d configuration of Ce^{3+} relative to the free ion value of 6.352 eV. $\epsilon_{cfs}(1, 3+, \mathrm{A})$ is the energy difference between the lowest and highest energy 5d states. $r(\mathrm{A})$ depends on the shape of the anion polyhedron that coordinates Ce^{3+} and it determines the fraction of ϵ_{cfs} that contributes to the red-shift.

$D(n, Q, \mathrm{A})$ is almost independent of n and equation (1) holds; this implies that the 5d crystal field splitting and centroid shift are almost the same for each lanthanide ion. This was suggested before [3–5], and first experimental evidence was provided by a systematic study on the fd transitions in 11 different trivalent lanthanides in CaF_2, $LiYF_3$, and YPO_4 [6–8]. There it was found that the centroid shift remains quite constant but the crystal field splitting decreases gradually by 10% with decreasing size of the lanthanide ion in going from Ce^{3+} to Tm^{3+}. Such change in the crystal field splitting causes dispersion of $D(Q, \mathrm{A})$ with the type of lanthanide and limits the predictive power of equation (1).

Red-shift, crystal field splitting, and centroid shift are known for Ce^{3+} in many compounds [2, 9–12]. To explore whether the crystal field interaction changes with the type of lanthanide ion, the information on the 5d level energies of Pr^{3+} and Tb^{3+} is compared with that on Ce^{3+}. Pr^{3+} is next to Ce^{3+} in the lanthanide series and has almost the same ionic radius as Ce^{3+} [13]. For this ion, corrections to equation (1) are not expected to be necessary. Since much spectroscopic information is available on Tb^{3+} and because it is ≈10 pm smaller than Ce^{3+}, Tb^{3+} is the most suitable lanthanide for use in testing whether corrections are needed for the smaller lanthanides.

Tb^{3+} is also of special interest because the isotropic exchange interaction between the 5d electron spin and the total spin of the electrons in the $4f^{n-1}$ core is maximal. It leads to a difference of ≈1 eV between the energy of the first spin allowed and first spin forbidden fd transition. Recently Shi and Zhang showed [14] that the exchange splitting of Tb^{3+} in compounds depends on the size of the nephelauxetic effect. Such change affects the red-shift $D(8, 3+, \mathrm{A})$ of Tb^{3+} differently to the red-shift $D(1, 3+, \mathrm{A})$ of Ce^{3+}; dispersions in red-shift values are then unavoidable.

This work is organized as follows. First the theory of the $4f^{n-1}5d$ configuration of the lanthanides is reviewed, and different schemes of coupling between 5d electrons and $4f^{n-1}$ electrons are considered. On the basis of the decoupled scheme, a simple model is introduced that reproduces the profile of the $4f^2 \rightarrow 4f^15d$ excitation spectrum of Pr^{3+}. Two energy shift operations need to be performed on the known fd excitation spectrum of Ce^{3+}.

The exchange interaction is accounted for by introducing an additional energy shift operation. It allows one to reproduce the $4f^8 \rightarrow 4f^75d$ excitation spectrum of the spin allowed and spin forbidden transitions in Tb^{3+} from the known spectrum of Ce^{3+}. Data on Tb^{3+} are collected from existing literature, and with the predictions from the 'shift model' the Tb^{3+} spectra are reanalysed. It will be shown that the energy difference between the spin forbidden fd and the spin allowed fd transition decreases with the amount of covalency between the 5d orbital and anion ligands. The implications for the accuracy of equation (1) are discussed, and finally the variation of the exchange splitting with the type of lanthanide and the type of host crystal is treated.

2. Theory

The electronic part of the Hamiltonian describing the $4f^{n-1}5d^1$ configuration is written as [15–17]

$$H = H_{ff}^{C} + H_{ff}^{ex} + H_{fd}^{C} + H_{fd}^{ex} + V_f + V_d + H_f^{so} + H_d^{so} \tag{3}$$

where H_{ff}^{C} and H_{ff}^{ex} are the Coulomb and exchange interactions between the electrons in the $4f^{n-1}$ configuration. H_{fd}^{C} and H_{fd}^{ex} are the same interactions between 5d electrons and $4f^{n-1}$ electrons. V_f and V_d describe the interaction of 4f electrons and 5d electrons with the crystal field. H_f^{so}, and H_d^{so} are the spin–orbit interactions of the f and d electrons.

In the case of Ce^{3+} all terms involving f electrons are absent, and then the crystal field splitting ϵ_{cfs} and the centroid shift ϵ_c are determined by V_d and

$$H_d^{so} = \zeta_d \vec{l}_d \cdot \vec{s}_d \tag{4}$$

where ζ_d is the 5d spin–orbit interaction parameter. In compounds with sites of low symmetry, the effect of the 5d spin–orbit interaction is quenched by the crystal field splitting, and then V_d is the only remaining interaction.

For the other lanthanides one may safely ignore V_f because the interaction between 4f electrons and the crystal field is very small [16]. If also the interactions between 5d and $4f^{n-1}$ electrons is ignored, we arrive at the decoupled scheme

$$H_0 = H_{ff}^{C} + H_{ff}^{ex} + H_f^{so} + V_d. \tag{5}$$

The levels of $4f^{n-1}5d^1$ are written as $4f^{n-1}[^{2S+1}L_J]5d_i$, i.e., as a product of the eigenstates of the $4f^{n-1}$ configuration with the eigenstates of $5d^1$. The $^{2S+1}L_J$ levels are determined by the first three terms in equation (5). The energy of $5d_i$, where the index $i = 1, 2, \ldots, 5$ denotes the five levels in order of increasing energy, are determined by V_d.

The isotropic exchange interaction between the 5d electron spin $\vec{s}_d$ and the total spin $\vec{S}_f$ of the $4f^{n-1}$ electrons is given by [15]

$$H_{fd}^{ex} = -2J_0 \vec{s}_d \cdot \vec{S}_f \tag{6}$$

with J_0 as the exchange interaction strength. In the case of high values for $\vec{S}_f$, like in Eu^{3+}, Gd^{3+}, Tb^{3+}, Sm^{2+}, Eu^{2+}, and Gd^{2+}, H_{fd}^{ex} is stronger than H_f^{so}. Ignoring H_f^{so}, the levels of $4f^{n-1}5d^1$ may be written as $4f^{n-1}[^{2S_f+1}L_f]5d_i$[HS] and $4f^{n-1}[^{2S_f+1}L_f]5d_i$[LS] where the attachment [HS] and [LS] indicates whether the 5d electron spin is parallel (high spin) or anti-parallel (low spin) to $\vec{S}_f$.

Figure 1 shows the energy level scheme of the $4f^7[^8S]5d$ configuration of free Gd^{2+} and free Tb^{3+} [18, 19]. The average energy of the levels is chosen as the zero of energy. The most important interaction is H_{fd}^{ex} causing a separation of $8J_0$ between the high spin [HS] ^9D_J and the low spin [LS] ^7D_J multiplets. The spin–orbit coupling causes the additional Landé interval splitting of ^9D_J and ^7D_J. The exchange and spin–orbit splitting are larger in Tb^{3+} which is related to the 18 pm smaller size of Tb^{3+}.

In compounds the orbital angular momentum of the 5d electron is quenched and then H_f^{so} commutes with the total angular momentum [15, 16]:

$$J' = S_f + s_d + L_f \equiv S' + L_f, \tag{7}$$

with

$$H_f^{so} = \zeta \vec{S}' \cdot \vec{L}_f. \tag{8}$$

In this $(S', L_f)J'$ coupling scheme, the energy levels are written as $4f^{n-1}[^{2S_f+1}L_f]5d_i[HS]_{J'}$ and $4f^{n-1}[^{2S_f+1}L_f]5d_i[LS]_{J'}$. For Tb^{3+} and Gd^{2+} a particularly simple situation is obtained because $L_f = 0$ and the Landé splitting of the ^9D and ^7D levels vanishes.

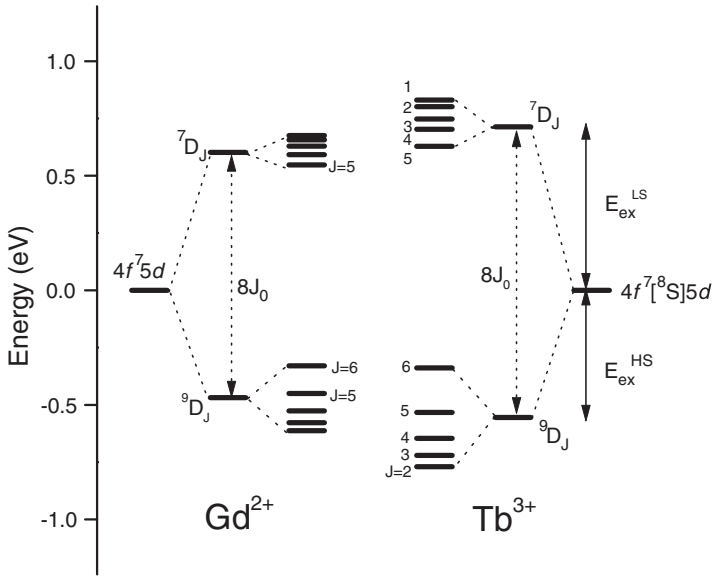

Figure 1. The energy level scheme showing the effect of the exchange splitting and spin–orbit splitting on the $4f^7[^8S]5d$ states of free Gd^{2+} and free Tb^{3+}.

$(S', L_f)J'$ coupling can be used for the lanthanides up to Tb^{3+} and Gd^{2+}. Proceeding further to the end of the lanthanide series, the exchange interaction decreases but the spin–orbit interaction becomes much stronger. For lanthanides such as Tm, Yb, Lu, the $(J_f j_d)J'$ coupling scheme is more appropriate [20, 21]. First the spin and angular momentum of the $4f^{n-1}$ core couple to J_f and those of the 5d electron couple to j_d. The J_f and j_d coupling is performed next leading to further substructure in the level scheme.

3. The shift model

In this section a model for generating the $4f^n \rightarrow 4f^{n-1}5d$ excitation or absorption spectra of trivalent lanthanides is presented. It is a practical model meant to roughly predict or interpret fd excitation spectra without entering into too much theoretical detail. Information on the energy of each 5d level of Ce^{3+} and on the $4f^{n-1}$ level energies of the lanthanide is needed as input. By means of energy shift operations performed on these 5d energies the model, hereafter called the 'shift model', constructs the $4f^{n-1}5d$ energy level diagram for other lanthanides. One element of the shift model is already expressed by the red-shift $D(Q, A)$ in equation (1). With information on the energy of the lowest 5d level of Ce^{3+} in a compound, the first $4f^{n-1}5d$ level of other lanthanides can be predicted by applying the red-shift $D(Q, A)$.

One may choose the decoupled, the $(S', L_f)J'$, or the $(J_f, j_d)J'$ coupling schemes as the basis for the shift model. Figure 2 illustrates the shift model applied to Pr^{3+} in $LiYF_4$ using the decoupled scheme. The energies of the five $5d_i$ $(i = 1, \ldots, 5)$ levels of Ce^{3+} in $LiYF_4$ are shown in the left part of figure 2. In the case of Pr^{3+} one may simply shift the levels by $E_{Afree}(2, 3+) - E_{Afree}(1, 3+) = 1.52$ eV to obtain the 4f5d levels with the 4f electron occupying the $^2F_{5/2}$ ground state level. The crystal field splitting between the 5d levels is maintained because V_d for Pr^{3+} is assumed the same as for Ce^{3+}. We will denote this shift operation as Sh_d.

The electron remaining in $4f^1$ can also be found in the $^2F_{7/2}$ state leading to an additional set of five 4f5d levels at higher energy. This additional shift denoted as Sh_f is the same as

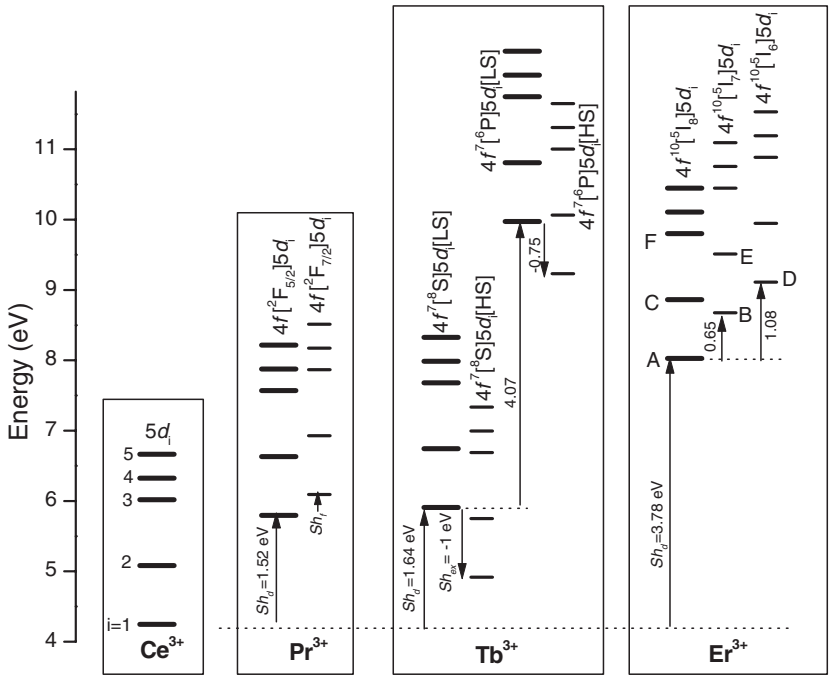

Figure 2. Experimental 5d level energies of Ce^{3+} in $LiYF_4$ and the level positions for Pr^{3+}, Tb^{3+}, and Er^{3+} generated by the shift model.

the difference between the $^2F_{5/2}$ and the $^2F_{7/2}$ level of the $4f^1$ core. It is 0.19 and 0.26 eV in the $4f^1$ configuration of La^{2+} and Ce^{3+}. For the $4f^15d$ configuration of Pr^{3+} we estimate a slightly larger spin–orbit splitting of ≈0.3 eV because of the contraction of the $4f^1$ core after fd excitation.

As an example, figure 3 shows the excitation spectra of df emission of Ce^{3+} and Pr^{3+} in $NaMgF_3$ [22]. The five bands of Ce^{3+} are nicely resolved. The shift operations Sh_d and Sh_f, illustrated by the set of vertical bars above the spectra, reproduce the main features, i.e., the position but also intensity of the Pr^{3+} excitation spectrum. The same was observed for Ce^{3+} and Pr^{3+} in $KMgF_3$ [22], and in $CaSO_4$, $SrSO_4$, and $BaSO_4$ [25], and in $LaPO_4$ [24].

The appropriate coupling scheme for Pr^{3+} is $(S', L_f)J'$ coupling resulting in three separate levels ($J' = 4, 3, 2$) for each $5d_i$ state instead of two. Usually, as in figure 3, the corresponding excitation bands are not resolved because of strong electron–phonon coupling and because of overlap with higher $5d_i$ states. Exceptions are provided by CaF_2, $LiYF_4$, and YPO_4 where the electron–phonon coupling is very weak and the energy separation between the $5d_1$ and the next higher non-degenerate $5d_i$ state is larger than the splitting between J' states. Van Pieterson *et al* [6, 7] found for these compounds two subbands at 0.17 and 0.45 eV higher energy than the first 4f5d band. In our notation the states can be written as $4f^1[^2F]5d_1[HS]_{4,3,2}$.

In those cases where (J_f, j_d) coupling is more appropriate, each $^{2S+1}L_J$ level of $4f^{n-1}$ defines a Sh_f operation. The Sh_f energies can be estimated from the Dieke diagram of the trivalent lanthanides [23]. For example, the fd excitation spectrum of Er^{3+} in $LiYF_4$ is well reproduced by $Sh_d = E_{Afree}(11, 3+) - E_{Afree}(1, 3+) = 3.78$ eV together with $Sh_f = 0$, 0.65, and 1.08 eV; see figure 2. The Sh_f values were taken as the same as the energy differences between the $^5I_8$, $^5I_7$, and $^5I_6$ states of the $4f^{10}$ configuration in free Ho^{3+} [23]. Within 0.15 eV the first five fd bands, denoted as A to F in figure 2, correspond with experiment [7].

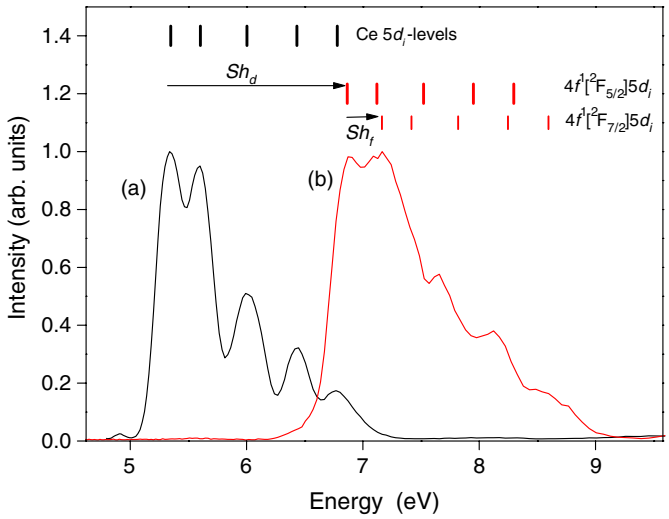

Figure 3. The 4f $\rightarrow$ 5d and 4f^2 $\rightarrow$ 4f^{1}5d excitation spectra of Ce^{3+} and Pr^{3+} luminescence in $NaMgF_3$. The vertical bars above the Pr^{3+} spectrum indicate Pr 5d level energies generated by the shift model from the Ce^{3+}5d energies.

(This figure is in colour only in the electronic version)

The lanthanide of special interest in this work is Tb^{3+}. With $Sh_d = E_{Afree}(8, 3+) - E_{Afree}(1, 3+) = 1.64$ eV the five main levels of the 4f^{7}5d configuration are obtained; see figure 2. The levels with the 4f^7 core in the ^{6}P state can be generated with $Sh_f = 4.07$ eV, i.e., the same energy difference as between ^{8}S and ^{6}P of the 4f^7 configuration in Gd^{3+}. Since this shift is always larger than the total crystal field splitting of the 5d levels, the 4f^7[^{6}P]5d$_i$ states are well separated from the five 4f^7[^{8}S]5d$_i$ states.

The effect of the isotropic exchange interaction can be accounted for by introducing a third type of shift operation. Performing $Sh_{ex} = -1$ eV on the 4f^7[^{8}S]5d$_i$[LS] states yields the 4f^7[^{8}S]5d$_i$[HS] states. We can do the same with the 4f^7[^{6}P]5d$_i$[LS] states. Because of the smaller $\vec{S}_f$ the splitting between [HS] and [LS] is $6J_0$ instead of $8J_0$, and then $Sh_{ex} \approx -0.75$ eV. Note that the transition to 4f^7[^{6}P]5d$_1$[HS] anticipated at 9.23 eV is the spin allowed one. The so-called J and J' bands observed by van Pieterson *et al* [26] in $LiYF_4$: Tb^{3+} at 9.47 and 9.32 eV are most probably related to this transition.

4. Results and discussion

There are two main points of interest in this work. (1) To what extent can the energy of the 4f^{n-1}5d$_i$ levels be predicted by applying the shift model to the known fd excitation spectrum of Ce^{3+}? (2) What are the causes for dispersion of $D(n, 3+, A)$ with n and how do they influence the predictive power of equation (1). We will treat two probable causes for dispersion.

(1) The ionic radius of the lanthanide ion decreases by 16 pm in going from La^{3+} to Lu^{3+} [13]. Unavoidably the lattice relaxation changes with the size of the lanthanide, and this affects the interaction V_d.

(2) The charge cloud expansion of the 5d orbital (nephelauxetic effect) and mixing with ligand orbitals (covalency) reduce the isotropic exchange interaction.

Such an effect was recently noticed for several Tb^{3+} doped compounds [14]. It is also a known phenomenon for the s^2 elements Tl^+, Pb^{2+}, Bi^{3+} where the exchange splitting between ^3P and ^1P terms of the sp excited configuration is strongly reduced in compounds [27].

We will focus on comparing the experimental fd excitation spectra of Pr^{3+} and Tb^{3+} with that of Ce^{3+}. Because of the relatively low energy of the 5d levels these are the most widely studied trivalent lanthanides. Furthermore, the spectroscopy of the $4f^{n-1}5d$ configuration is relatively simple for these lanthanides.

Data on Pr^{3+} and especially Tb^{3+} were critically (re)analysed using the shift model. Identification of the first two intense spin allowed and the first weak spin forbidden fd transition in Tb^{3+} is usually not problematic. However, there are the following uncertainties on how to assign the higher energy levels of the $4f^75d$ configuration:

(1) Figure 2 illustrates that when the energy difference between $5d_1$ and $5d_2$ is smaller than 0.75 eV, one may observe below the first $5d_1$[LS] state the spin forbidden transition to $5d_1$[HS] and $5d_2$[HS] states.
(2) One may not assume beforehand that the orbital angular momentum of the 5d electron is fully quenched in compounds. Although, this was suggested in several theoretical treatments [15–17], it has not been verified for Tb^{3+}. If the assumption does not hold, then the ^9D state splits further and more than one spin forbidden transition could be observed below the first spin allowed one.
(3) The exchange interaction J_0 may depend on the type of compound. The interaction may also be different for the higher $5d_i$ states.
(4) It is not known what intensities to expect for the spin forbidden transitions as compared to the spin allowed ones.

To analyse Tb^{3+} fd excitation spectra, the shift model combined with information on Ce^{3+} is used to assign the different bands observed, and vice versa the bands observed are used to verify to what extent the shift model holds. To test and illustrate the shift model, a spectroscopic study was done on Ce^{3+} and Tb^{3+} doped $LiLuSiO_4$. Figure 4 shows the excitation spectra of Ce^{3+} df emission at 400 nm and Tb^{3+} ff emission at 545 nm. The experimental techniques used can be found elsewhere [22]. The first three Ce^{3+} 5d excitation bands are found at 3.51, 3.91, and 4.08 eV. The other two, anticipated around 6.4 eV, are too weak to be detected. The fundamental absorption due to excitation of the SiO_4^{4-} groups starts at $E_{fa} = 7.15$ eV.

On lowering the temperature to 10 K (spectrum 2), the $5d_2$ and $5d_3$ bands narrow and can be resolved in the spectrum. Application of the shift operation $Sh_d = 1.69$ eV to the first three Ce^{3+} levels provides the Tb^{3+} $4f^7[^8S]5d_i$[LS] level energies. They agree with intense excitation bands observed at 5.23 and 5.64 eV. Note that the splitting between $5d_2$ and $5d_3$ is 0.023 eV smaller than for Ce^{3+} and the two bands are not resolved in spectrum (3). Probably the asymmetry on the high energy side of the 5.64 eV band indicates the presence of the $5d_3$ band. The 50 and 10 times weaker bands at 4.31 and 4.75 eV are attributed to the $5d_1$[HS] and the unresolved $5d_{2,3}$[HS] bands of Tb^{3+}. A shift operation $Sh_{ex} = -0.92$ eV on the [LS] Tb^{3+} bands reproduces nicely the energies of the observed high spin bands. Spectrum (4) measured with a higher wavelength resolution and longer photon counting time reveals a narrow Tb^{3+} $4f^8 \rightarrow 4f^8$ transition at 3.89 eV. The spin forbidden fd excitation bands are much wider and do not reveal any substructure.

Based on the $LiLuSiO_4$ data and data to be presented further on in this work, the following five conclusions are drawn:

(1) The Sh_d shift operation provides the main bands of Tb^{3+}.
(2) The exchange splitting between [HS] and [LS] bands is the same for each $5d_i$, and the [HS] levels can be found by using the Sh_{ex} shift operation.

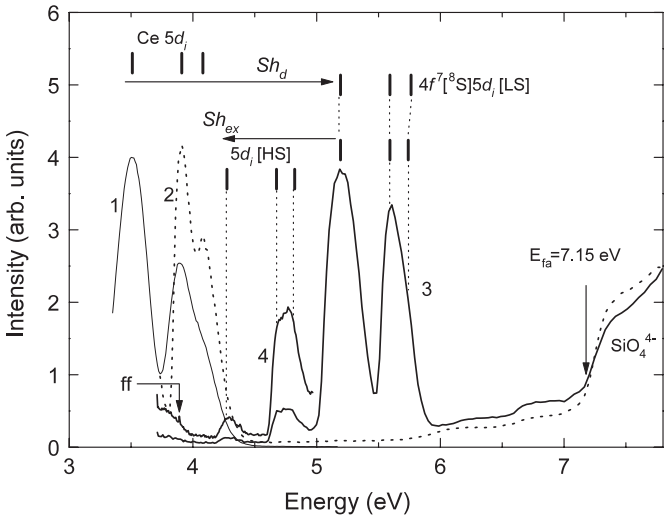

Figure 4. Excitation spectra of 400 nm Ce^{3+} df emission in $LiLuSiO_4$ at 295 K (spectrum (1)) and 10 K (spectrum (2)). Spectrum (3) is the excitation spectrum of 545 nm Tb^{3+} ff emission in $LiLuSiO_4$ at 10 K. Na salicylate was used to correct for the light source spectral profile. Spectrum (4) is like spectrum (3) but with longer counting time and smaller wavelength step size. The wavelength resolution is 0.3 nm. Vertical bars illustrate band positions generated by the shift model.

(3) The intensity of the transition to the $5d_1$[HS] level is 10–50 times weaker than that to the $5d_1$[LS] level.
(4) The intensity of the transition to the $5d_2$[HS] level is 5–10 times stronger than that to $5d_1$[HS].
(5) Only one single spin forbidden transition to $5d_1$[HS] is observed. The absence of a further splitting of $5d_1$[HS] confirms that the 5d angular momentum is quenched in compounds and that the H_f^{so} interaction, because $L_f = 0$, can be ignored for Tb^{3+}.

4.1. Presentation of data

A large part of the information on fd transitions in Ce^{3+}, Pr^{3+}, and Tb^{3+} together with references can be found in previous work [2, 9–12, 28]. Since the appearance of that work, more information has been retrieved from the literature. Not all data is presented; instead a subset of the most relevant data are tabulated. Table 1 for example compiles data on those compounds where both the $5d_1$[HS] and $5d_1$[LS] levels of Tb^{3+} were identified.

Figure 5 shows the energies of the first allowed fd absorption and df emission in Ce^{3+}, Pr^{3+}, and Tb^{3+} against that in Ce^{3+}. For this figure, the full collection of available data was used. When equation (1) holds, all data must fall on sets of parallel lines with unit slope. It applies best to Pr^{3+} where the energy difference between the fd transition in Pr^{3+} and that in Ce^{3+} averaged over $N = 110$ data points amounts to 1.51 ± 0.09 eV. Note that the ± 3 nm uncertainty in the absorption and emission wavelengths of Ce^{3+} and Pr^{3+} already accounts for the ± 0.08 eV error in the energy difference. Therefore, within experimental accuracy, equation (1) applies and $D(2, 3+, A) = D(1, 3+, A)$.

The allowed first fd transition in Tb^{3+} is on average ($N = 75$) at 1.66 ± 0.12 eV higher energy than that in Ce^{3+}. Like for Pr^{3+} the experimental uncertainty is ± 0.08 eV. In the following sections two causes for the additional dispersion of 0.08 eV leading to the overall dispersion of 0.12 eV are considered. (1) V_d for Tb^{3+} is different to that for Ce^{3+} leading to

Table 1. The energies (eV) of the first spin allowed $E^{sa}(8, 3+, A)$ and the first spin forbidden $E^{sf}(8, 3+, A)$ transitions of Tb^{3+} in compounds A. The intensity ratios I^{sf}/I^{sa} of the spin forbidden to spin allowed transitions in excitation spectra are specified, together with the Tb^{3+} concentration within brackets. $\Delta E_1^{ex} = E^{sa} - E^{sf}$. All energies are in electron volts.

Compound	E^{sf}	E^{sa}	ΔE_1^{ex}	I^{sf}/I^{sa}	References
CaF_2	4.79	5.77	0.980		[7, 37, 38]
$LiYF_4$	4.86	5.88	1.014	0.017 (1%)	[7, 39, 40]
Acetonitrile $(RECl_6)^{3-}$	4.56	5.30	0.740	0.02 (100%)	[41, 42]
Acetonitrile $(REBr_6)^{3-}$	4.46	5.12	0.663		[41, 42]
α-GdOF	4.77	5.51	0.742	0.07 (2%)	[43]
β-GdOF	4.40	5.17	0.769	0.06 (2%)	[43]
YOF	4.31	5.17	0.861	0.03 (5%)	[44]
$Y_3(SiO_4)_2Cl$	4.53	5.32	0.796	0.1 (4.3%)	[45]
LuOCl	3.88	4.75	0.876	0.027 (2%)	[46, 47]
ScOCl	4.13	4.88	0.749	0.014 (2%)	[46]
LaOBr	4.29	4.86	0.572	0.1 (7.5%)	[48–50]
YOBr	4.26	4.86	0.602	0.04 (5%)	[44]
LaOI	3.82	4.70	0.882	0.01 (0.6%)	[47, 51]
$CaSO_4$	4.86	5.82	0.959	0.023 (2%)	[52]
$Y_2O_2(SO_4)$	4.51	5.39	0.882		[53]
TbP_5O_{14}	4.82	5.71	0.889	0.32 (100%)	[54, 55]
LaP_3O_9	4.91	5.88	0.966	0.05 (5%)	[56]
GdP_3O_9	4.90	5.85	0.948	0.03 (5%)	[56]
$KTbP_4O_{12}$	4.77	5.74	0.971	0.33 (100%)	[55]
YP_3O_9	4.73	5.71	0.981	0.03 (5%)	[56]
$LaPO_4$	5.12	6.05	0.925	0.05 (4%)	[24, 56, 57]
$K_3La(PO_4)_2$	4.88	5.69	0.806	0.5 (20%)	[58, 59]
$GdPO_4$	5.00	6.02	1.019	0.04 (5%)	[56, 60]
$TbPO_4$	4.77	5.64	0.867	0.44 (100%)	[61]
$K_3Tb(PO_4)_2$	4.70	5.61	0.914	0.3 (100%)	[55, 59, 62]
β-$Na_3Gd(PO_4)_2$	4.71	5.49	0.772	0.08 (0.5%)	[63]
YPO_4	4.66	5.56	0.899	0.07 (0.11%)	[7, 56, 64]
$LuPO_4$	4.70	5.54	0.839		[64]
$ScPO_4$	4.56	5.44	0.880		[64]
Aqueous $[Tb(OH_2)_8]^{3+}$	4.71	5.66	0.947		[65–67]
$BaLaB_9O_{16}$	5.00	5.99	0.990	0.05 (10%)	[55, 68]
$BaGdB_9O_{16}$	5.06	5.99	0.929	0.06 (20%)	[68, 69]
LaB_3O_6	5.39	6.20	0.809	0.016 (5%)	[56, 70]
$Ca_3(BO_3)_2$	4.40	5.19	0.791	0.02 (0.3%)	[71, 72]
$LaBO_3$	4.61	5.49	0.877	0.033 (20%)	[44, 56]
$GdAl_3(BO_3)_4$	4.71	5.61	0.896		[73]
$TbAl_3(BO_3)_4$	4.63	5.59	0.959	0.17 (100%)	[74, 75]
$GdBO_3$	4.41	5.28	0.864	0.15 (20%)	[44, 56, 76, 78]
$TbBO_3$	4.44	5.28	0.832	0.30 (100%)	[61]
$Na_6Gd(BO_3)_3$	4.08	4.81	0.727	0.085	[79]
YBO_3	4.38	5.25	0.873	0.08 (20%)	[56, 78, 80]
Calcite $LuBO_3$	4.40	5.34	0.948		[81]
$ScBO_3$	4.29	5.19	0.898	0.06 (0.13%)	[44, 76, 78, 81]
$InBO_3$	4.40	5.28	0.879	0.05 (0.11%)	[77, 81]
β-$Y_2Si_2O_7$	4.35	5.23	0.881	0.074	[82, 83]
Mg_2SiO_4	4.16	5.08	0.921	0.07 (9%)	[55, 84]
$Gd_3Mg_2GaGe_2O_{12}$	3.51	4.31	0.793	0.03	[85]
$Y_3Mg_2GaGe_2O_{12}$	3.47	4.28	0.802	(1%)	[85]
$LiLuSiO_4$	4.29	5.21	0.919	0.019	This work

Table 1. (Continued.)

Compound	E^{sf}	E^{sa}	ΔE_1^{ex}	I^{sf}/I^{sa}	References
X1-Gd_2SiO_5:(Ce2)	4.01	4.96	0.947	0.083 (2%)	[86]
X1-Y_2SiO_5	4.32	5.08	0.761	0.07 (0.12%)	[87, 88]
X2-Y_2SiO_5:(Ce1)	4.29	5.15	0.855	0.09	[83, 88–90]
$Y_2Ca_2(Si_2O_7)O_2$	4.35	5.28	0.926	0.05 (5%)	[44]
$Mg_2Y_8(SiO_4)_6O_2$:(6h)	4.51	5.23	0.723	0.06 (2.7%)	[91]
$CaAl_2O_4$:Ce2	4.38	5.04	0.659	0.49 (1%)	[92, 93]
$SrLaGa_3O_7$	4.38	5.17	0.785	0.19 (80%)	[94]
$GdAlO_3$	4.90	5.66	0.761	0.20 (2%)	[95, 96]
$Gd_3Ga_5O_{12}$	3.95	4.63	0.678	0.31 (6%)	[97]
$Y_3Al_5O_{12}$	3.86	4.54	0.679	(0.03) (1%)	[44, 98, 99]
$Y_3Al_4GaO_{12}$	3.88	4.63	0.752		[98]
$Y_3Al_3Ga_2O_{12}$	3.91	4.64	0.732	0.09	[98]
$Y_3Al_2Ga_3O_{12}$	3.97	4.68	0.705	—	[44, 98]
$Y_3AlGa_4O_{12}$	3.99	4.68	0.692	0.11	[98]
$Y_3Ga_5O_{12}$	4.00	4.70	0.697	0.24 (5%)	[44, 98, 100]
$La_2Hf_2O_7$	4.43	5.10	0.674	0.10 (1%)	[101]
$SrLa_2BeO_5$	4.07	4.77	0.704	0.16 (1%)	[102]
$LiSr_2YO_4$	3.35	3.88	0.524	0.15 (10%)	[103]
C-Lu_2O_3	3.54	4.05	0.509	0.004 (1%)	[104]

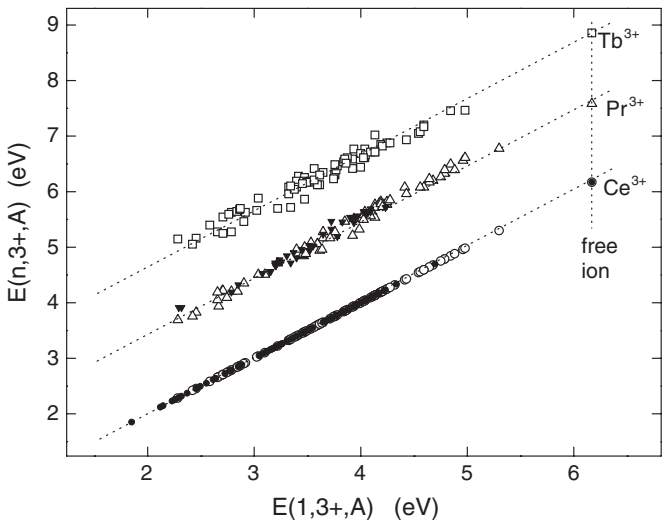

Figure 5. $E(n, 3+, A)$ for Ce^{3+}, Pr^{3+}, and Tb^{3+} against $E(1, 3+, A)$ for Ce^{3+}. Open symbols are data on f → d absorption transitions and solid symbols data on d → f emission transitions. For presentation purposes, the data for Tb^{3+} are offset by 1.0 eV. Dashed lines have unit slope.

different crystal field splitting and centroid shift. (2) The exchange interaction H_{fd}^{ex} depends on the type of compound.

The shift model works for the first allowed fd transition in Tb^{3+}. To test the model for the transitions to higher 5d levels and the spin forbidden ones, data were collected on the energies of these transitions also. Table 2 compiles the energies of the five $5d_i$ levels of Ce^{3+}. With the shift model applied to these data, $4f^8 \rightarrow 4f^7 5d$ excitation spectra of Tb^{3+} in compounds were interpreted. The energies of the $4f^7[^8S]5d_i$[LS] and $4f^7[^8S]5d_i$[HS] identified are compiled

Table 2. Energies E_i ($i = 1, \ldots, 5$) of the $5d_i$[HS] and $5d_i$[LS] states of Ce^{3+} and Tb^{3+} in compounds in electron volts.

Compound	Ln	E_5	E_4	E_3	E_2	E_1
LaF_3	Ce	6.39	5.96	5.69	5.30	4.98
	Tb [LS]	8.09	7.64	7.24	6.87	6.47
	Tb [HS]	7.06	6.64	6.17	—	—
YF_3	Ce	6.39	6.11	5.74	5.19	4.84
	Tb [LS]	8.05	7.75	7.47	6.91	6.46
	Tb [HS]	7.07	6.69	6.29	5.82	—
$LiYF_4$	Ce	6.67	6.33	6.02	5.08	4.25
	Tb [LS]	8.21	8.05	7.75	6.81	5.88
	Tb [HS]	—	—	—	—	4.86
LaP_3O_9	Ce	6.39	6.05	5.41	4.68	4.28
	Tb [LS]	—	—	7.07	6.25	5.88
	Tb [HS]	—	6.72	5.96	5.22	4.91
$LaPO_4$	Ce	6.02	5.79	5.19	4.84	4.54
	Tb [LS]	—	—	6.88	6.36	6.05
	Tb [HS]	6.70	6.52	5.82	5.49	5.12
YPO_4	Ce	6.11	5.51	5.21	4.96	3.85
	Tb [LS]	7.70	7.17	6.93	6.74	5.56
	Tb [HS]	—	6.20	5.93	5.71	4.66
LaB_3O_6	Ce	6.08	5.66	5.04	4.77	4.59
	Tb [LS]	—	7.40	6.67	6.39	6.20
	Tb [HS]	—	—	—	5.66	5.39
$LaMgB_5O_{10}$	Ce	6.14	5.51	5.19	4.82	4.56
	Tb [LS]	—	7.17	6.89	6.39	6.08
	Tb [HS]	—	—	—	—	—
$LaBO_3$	Ce	5.77	5.34	5.15	4.66	3.76
	Tb [LS]	—	—	6.70	6.33	5.49
	Tb [HS]	—	6.11	5.82	—	4.61
YBO_3	Ce	6.20	5.66	5.06	3.67	3.47
	Tb [LS]	—	—	6.74	5.44	5.25
	Tb [HS]	—	—	5.90	4.58	4.38
Calcite $LuBO_3$	Ce	6.81	6.42	4.09	3.82	3.65
	Tb [LS]	—	—	—	—	5.34
	Tb [HS]	—	—	4.77	4.56	4.40
$ScBO_3$	Ce	6.74	6.46	3.88	3.62	3.46
	Tb [LS]	—	—	—	—	5.19
	Tb [HS]	—	—	4.71	4.46	4.29
Mg_2SiO_4	Ce	—	—	—	3.85	3.32
	Tb [LS]	—	—	6.36	5.56	5.08
	Tb [HS]	—	—	—	4.68	4.16
$LiLuSiO_4$	Ce	—	—	4.16	3.91	3.56
	Tb [LS]	—	—	5.71	5.61	5.21
	Tb [HS]	—	—	4.77	4.71	4.29
$GdAlO_3$	Ce	5.39	5.06	4.48	4.32	4.04
	Tb [LS]	—	—	—	5.98	5.66
	Tb [HS]	—	—	—	5.23	4.90
$Y_3Al_5O_{12}$	Ce	6.05	5.51	4.75	3.65	2.71
	Tb [LS]	—	—	—	5.45	4.54
	Tb [HS]	—	—	5.99	—	3.86

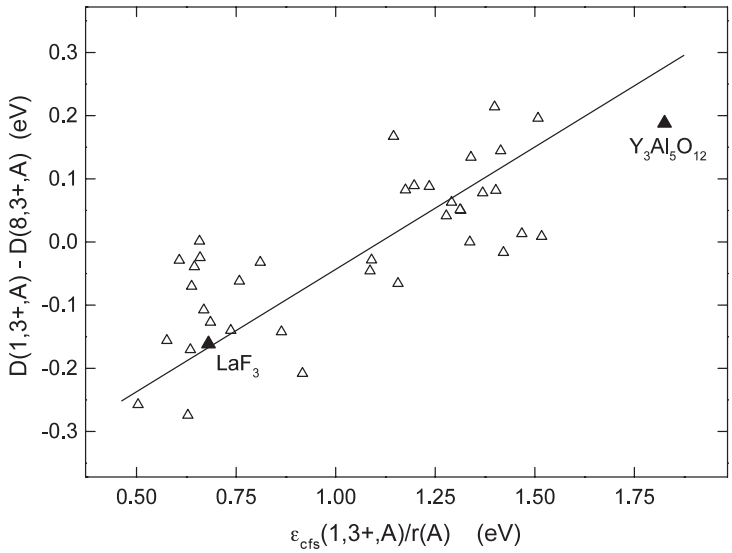

Figure 6. The difference between the Ce^{3+} 5d red-shift $D(1, 3+, A)$ and the Tb^{3+} 5d red-shift $D(8, 3+, A)$ as a function of the crystal field splitting contribution, $\epsilon_{cfs}(1, 3+, A)/r(A)$, to the Ce^{3+} red-shift.

in table 2. The literature on the Ce^{3+} data can be found in [2, 10–12] and references therein. The Tb^{3+} data on LaF_3 and YF_3 are from [29, 30] and those on $LaMgB_5O_{10}$ are from [31]. For other Tb^{3+} data the same sources as cited in table 1 were used.

4.2. Deviations from the shift model due to V_d

Crystal field splitting is caused by exchange (Pauling repulsion) and Coulomb interaction between 5d electron and anion ligands. Suppose Ce^{3+} is replaced by the smaller Tb^{3+} ion and lattice relaxation does not occur. The Coulomb and exchange interaction is less and consequently V_d and the crystal field splitting decrease. Although lattice relaxation partly cancels this effect, smaller crystal field splitting is still expected for Tb^{3+}. For CaF_2, YPO_4, and $LiYF_4$ van Pieterson *et al* [6, 7] found that the 5d crystal field splitting of Tb^{3+} is 5% smaller than that of Ce^{3+}. A 9% decrease was observed for the even smaller lanthanides Tm^{3+} and Yb^{3+}.

A crystal field splitting that depends on the size of the lanthanide ion affects the red-shift $D(3+, A)$; see equation (2). $D(n, 3+, A)$ then depends slightly on n and dispersion of the data in figure 5 is introduced. Figure 6 shows the difference between the red-shifts in Ce^{3+} and in Tb^{3+} against $\epsilon_{cfs}(1, 3+, A)/r(A)$. A clear correlation exists. For compounds with large crystal field splitting, like in $Y_3Al_5O_{12}$ with the garnet structure, $D(1, 3+, A) - D(8, 3+, A) > 0$.

For compounds providing a large lattice site for Tb^{3+} another effect may occur. When the anion coordination number is large ($\geqslant 8$) and the crystal field splitting small, lattice relaxation distorts the shape of the anion coordination polyhedron which may lead to augmented crystal field splitting. In that case, $D(1, 3+, A) - D(8, 3+, A)$ can be smaller than zero. This is the situation in LaF_3. The assignment of bands in table 2 indicates that the Tb^{3+} crystal field splitting is 13% larger in LaF_3 than the splitting for Ce^{3+}. The variation of the crystal field splitting with the size of the lanthanide is now regarded as a main contribution to the dispersion from equation (1).

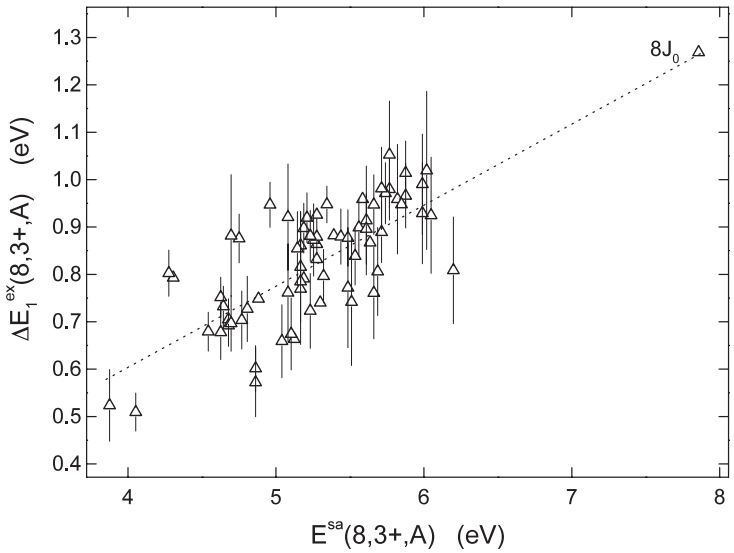

Figure 7. The relation between the exchange splitting $\Delta E_1^{\rm ex}$ and the energy $E^{\rm sa}(8, 3+, A)$ of the $4f^7[^8S]5d_1[LS]$ level in Tb^{3+}.

4.3. The deviations from the shift model due to H_{fd}^{ex}

The exchange splitting $\Delta E_1^{\rm ex}$, defined as the energy difference between $5d_1[LS]$ and $5d_1[HS]$, is shown in figure 7 against the energy $E^{\rm sa}(8, 3+, A)$ of the first spin allowed transition in Tb^{3+}. One observes a clear decrease with smaller $E^{\rm sa}(8, 3+, A)$. The data extrapolate to the value of $8J_0 = 1.27$ eV of the free ion. Further analysis reveals that $\Delta E_1^{\rm ex}$ does not correlate with the 5d crystal field splitting, but it does correlate with the size of the centroid shift. Figure 8 shows $\Delta E_1^{\rm ex}$ against the centroid shift of the Ce^{3+} 5d configuration which can be calculated from the Ce^{3+} data in table 2. An almost linear relationship is observed that again extrapolates to the value $8J_0 = 1.27$ eV for free Tb^{3+}.

Another way to demonstrate a relation between the exchange splitting and type of compound is via the so-called spectroscopic polarizability $\alpha_{\rm sp}$ of anions. This parameter is a measure for the amount of covalency between 5d and anion ligands and for the correlated motion of 5d electrons with ligand electrons which are the two most important contributions to the centroid shift of the 5d configuration [2]. It was recently found that $\alpha_{\rm sp}$ has a very simple relationship with the mean value $\chi_{\rm av}$ of the electronegativity of the cations in the compound [32]:

$$\alpha_{\rm sp} = \alpha_0 + \frac{b}{\chi_{\rm av}^2} \tag{9}$$

where α_0 is 0.33×10^{-30} m^3 and 0.15×10^{-30} m^3 for oxygen and fluorine, respectively. b is the susceptibility of the anion to change in its polarizability by binding to cations. It is 4.8×10^{-30} m^3 and 0.96×10^{-30} m^3 for oxygen and fluorine, respectively. $\chi_{\rm av}$ is defined as [32]

$$\chi_{\rm av} = \frac{1}{\gamma N_{\rm a}} \sum_i^{N_{\rm c}} z_i \chi_i \tag{10}$$

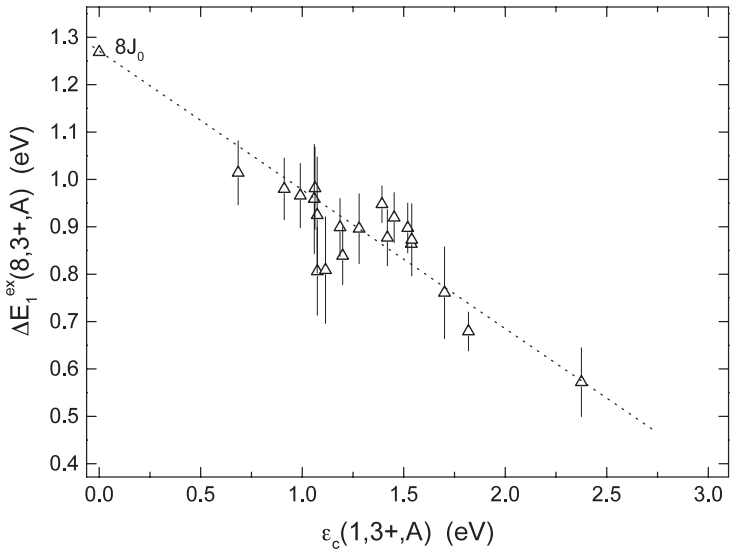

Figure 8. The exchange splitting $\Delta E_1^{\rm ex}$ against the centroid shift $\epsilon_{\rm c}(1, 3+, {\rm A})$ of the 5d configuration of Ce^{3+} in compounds.

where $N_{\rm a}$ is the number of anions in the compound formula. The summation is over all $N_{\rm c}$ cations where $-\gamma$ and z_i are the charges of the anion and the cation i. χ_i is the electronegativity of cation i as compiled by Allred [33].

Figure 9 shows the exchange splitting in Tb^{3+} in fluoride and oxide compounds against $\alpha_{\rm sp}$ calculated with equations (9) and (10). This much larger collection of data follows the same pattern as in figure 8. Shi and Zhang [14] recently related the exchange splitting observed for Tb^{3+} in eight different compounds to Jörgensen's nephelauxetic $h_{\rm e}$ parameter [34], and found a linear relationship:

$$\Delta E_{\rm ex}(8, 3+, {\rm A}) = 1.09 - 0.37 h_{\rm e}\ {\rm eV} \tag{11}$$

where the parameter $h_{\rm e}$ was calculated from the covalency between Tb and anions and from the polarizability of the bonds [14]. Relation (11) is very similar to that in figure 9. This is not too surprising since $\alpha_{\rm sp}$ and $h_{\rm e}$ are related parameters and more or less proportional to each other [35].

Because the size of the exchange splitting depends on the type of compound whereas in Ce^{3+} the exchange splitting is absent, red-shift values $D(n, 3+, {\rm A})$ cannot be constant with n and dispersion is unavoidable. Figure 10 shows the energy of the transition to $5d_1$[HS] and $5d_1$[LS] of Tb^{3+}. The reduction of exchange splitting is seen as a less than unit slope of the line through the $5d_1$[HS] data. Fortunately, the data on $5d_1$[LS] still follow a line of unit slope. It means that the reduction of the exchange splitting does not affect the red-shift of the $5d_1$[LS] level. However, it does reduce the red-shift of $5d_1$[HS]. Note that the data on the [HS] and [LS] $5d_1$ levels of Tb^{3+} extrapolate to the barycentre of the ^9D_J (6.588 eV) and ^7D_J (7.857 eV) states of free Tb^{3+}. This provides additional evidence for the quenching of the orbital momentum of the 5d electron due to the large 5d crystal field splitting in compounds. It also evidences that the $(S', L_{\rm f})J'$ coupling scheme applies for Tb^{3+}.

Summarizing, it is found that equation (1) with $E_{\rm Afree}\ (n, 3+) = 6.118$, 7.625, and 7.780 eV applies to Ce^{3+}, Pr^{3+}, and Tb^{3+}, respectively. Within the experimental accuracy of ± 0.08 eV, $D(1, 3+, {\rm A}) = D(2, 3+, {\rm A})$. The main reason that $D(8, 3+, {\rm A})$ may deviate

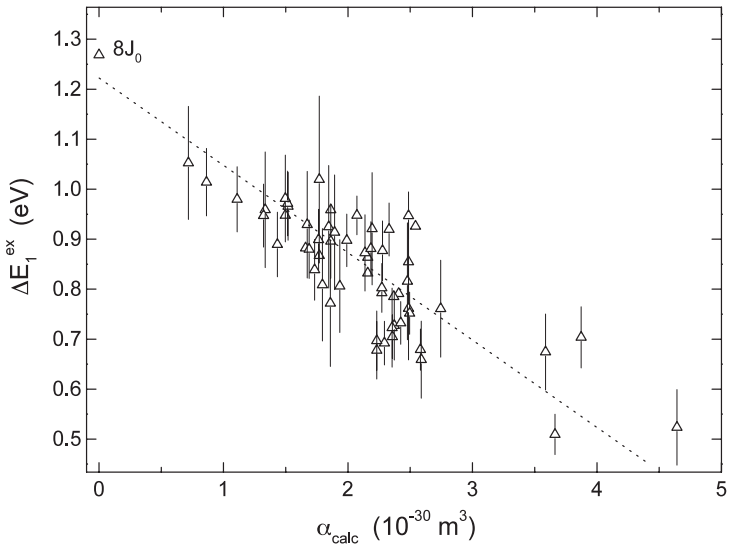

Figure 9. The exchange splitting $\Delta E_1^{\rm ex}$ against the calculated spectroscopic polarizability $\alpha_{\rm sp}$ of the anions in the compound.

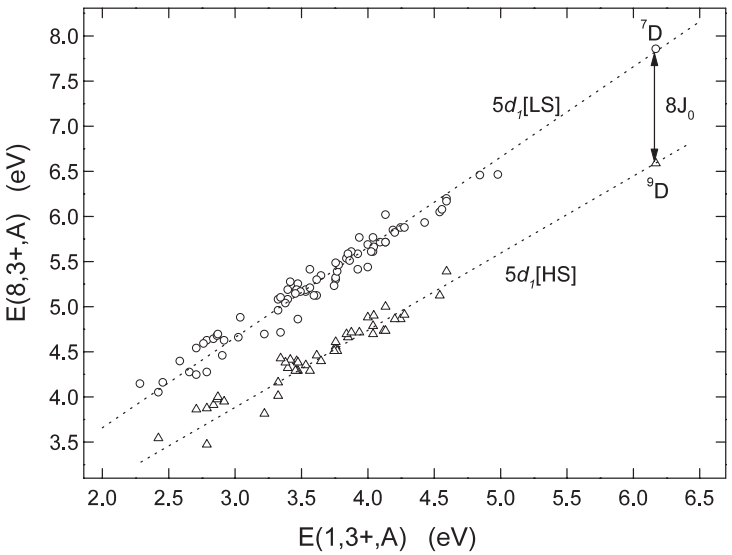

Figure 10. The energy of the first spin allowed and the first spin forbidden transition in Tb^{3+} against the energy of the first fd transition in Ce^{3+}. The dashed line through the [LS] data has unit slope, and that through the [HS] data has slope 0.85.

slightly but significantly from $D(1, 3+, A)$ is the smaller size of Tb^{3+}. The lattice relaxation is different to that for Ce^{3+}, and this influences the crystal field interaction $V_{\rm d}$. The reduction of $H_{\rm fd}^{\rm ex}$ in compounds mainly affects the energy of the $5d_i$[HS] state in Tb^{3+} and not that of the $5d_i$[LS] state.

The reduction of $H_{\rm fd}^{\rm ex}$ is attributed to mixing of the 5d orbital with anion ligand orbitals. It reduces the spin purity of the state and therefore the size of the exchange splitting in equation (6).

One then expects also an increase of the oscillator strength of the 'spin forbidden' transitions relative to that of the 'spin allowed' ones. To test this, the intensity ratio I^{sf}/I^{sa} between the $5d_1$[HS] and $5d_1$[LS] bands was determined and the data are compiled in table 1. Conclusive evidence is difficult to obtain because the oscillator strength also depends on other properties such as the site symmetry. Furthermore, the ratio I^{sf}/I^{sa} depends on the Tb^{3+} concentration. Nevertheless, I^{sf}/I^{sa} is about 0.02 in fluorides and in phosphates with strongly bonded anion electrons. In silicates and aluminates where bonding is weaker, the ratio tends to increase to values between 0.05 and 0.10.

What appears very clearly from the data is an increase in the oscillator strength for the transitions to the higher $5d_i$[HS] states as compared to transitions to $5d_1$[HS]. This can already be seen in figure 4 where the $5d_2$[HS] transition is ten times stronger than the $5d_1$[HS] transition. The same is generally observed in other compounds also. For the even higher $5d_i$ states, the spin forbidden transitions are often of comparable intensity to the spin allowed ones. Only by using the shift model and information available on Ce^{3+} can a distinction between the spin forbidden and spin allowed bands then be made.

4.4. Generalization to other lanthanides

The shift model and equation (1) work very well for Pr^{3+} and with somewhat larger error bars also for the smaller Tb^{3+} ion. For the even smaller lanthanides such as Tm^{3+} and Lu^{3+} the error is likely to increase further.

$\vec{S}_f$ reduces from 7/2 for Tb^{3+} to 1/2 for Yb^{3+}. Assuming that $J_0(n, 3+, A)$ does not depend on n and A, the splitting between the $5d_1$[HS] and $5d_1$[LS] states then decreases from $8J_0$ to $2J_0$. However, J_0 is not a constant. Figure 11 shows the estimated $J_0(n, 2+, \text{free})$ values for the free divalent lanthanides. The estimates were made by means of a parabolic fit through $J_0(n, 2+, \text{free})$ values reported for Ce^{2+} (0.21 eV), Pr^{2+} (0.20 eV), Tm^{2+} (0.17 eV), and Yb^{2+} (0.164 eV) in Yanase [16] and values for Eu^{2+} (0.135 eV) and Gd^{2+} (0.133 eV) from Spector and Sugar [19] and Callahan [18]. Since $J_0(8, 3+, \text{free})$ in Tb^{3+} is 19% larger than $J_0(8, 2+, \text{free})$ in Gd^{2+}—see figure 1—we assume for each lanthanide $J_0(n, 3+, \text{free}) = 1.19J_0(n, 2+, \text{free})$.

Figure 11 shows the energies E^{ex}_{HS} and E^{ex}_{LS} calculated with equation (6) for trivalent lanthanides. E^{ex}_{HS} is the energy by which the high spin states are lowered, and E^{ex}_{LS} is the energy by which the low spin states are raised due to the exchange interaction; see figure 1. For free ions, starting from Tb^{3+} with $n = 8$ and going up to Lu^{3+} with $n = 14$, the total exchange splitting decreases from $8J_0 = 1.27$ to $2J_0 = 0.41$ eV. In compounds, H^{ex}_{fd} is further reduced by at least 25%; see figure 9. One then expects the exchange splitting to decrease from 0.95 eV for Tb^{3+} towards 0.31 for Lu^{3+}. Such a trend is indeed observed experimentally [7, 28, 36]. However, the situation with the spin forbidden transitions in the heavy lanthanides is more complicated than that in Tb^{3+}. L_f is non-zero and this leads within the $(S', L_f)J'$ coupling scheme to more then one $5d_i$[HS] level. In Dy^{3+}, for example, two $5d_1$[HS] states are observed below the $5d_1$[LS] state [7].

5. Summary and conclusions

fd excitation spectra of Ce^{3+}, Pr^{3+}, and Tb^{3+} luminescence in compounds were gathered and reanalysed. Some of the data obtained on the energy of the $4f^{n-1}5d$ levels are compiled in tables 1 and 2. A method has been introduced that generates the energies of the main $4f^{n-1}5d$ levels in Pr^{3+} and Tb^{3+} in a compound from the known energies of the five 5d levels of Ce^{3+} in that same compound. The method is based on the assumption that the crystal field splitting

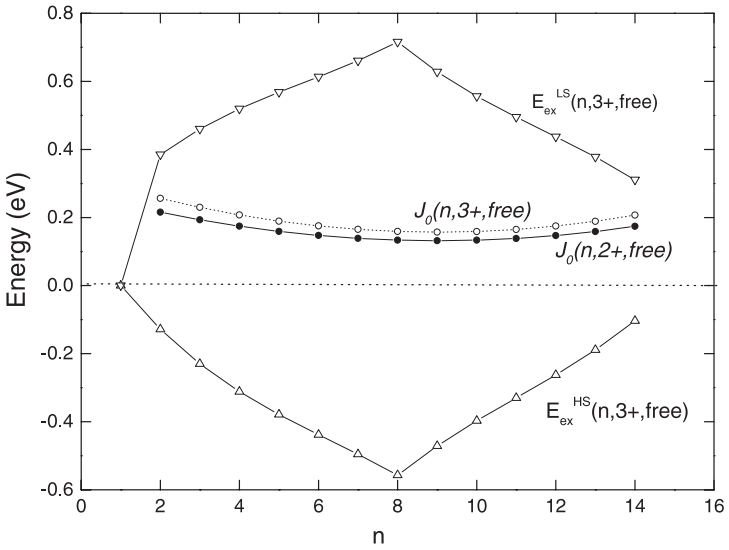

Figure 11. The exchange interaction parameter $J_0(n, Q, \mathrm{A})$ for the ◯ trivalent ($Q = 3+$) and ◇ divalent ($Q = 2+$) free lanthanide ions (A = free). ▽: the exchange interaction energy ($E^{\mathrm{ex}}_{\mathrm{LS}}$) of the low spin states; ▽: that ($E^{\mathrm{ex}}_{\mathrm{HS}}$) for the high spin states.

and centroid shift of the 5d levels, i.e., the interaction V_{d} in equation (3), are the same for each lanthanide ion. An upward shift by an amount $\mathrm{Sh_d}$ of the energy of each of the five 5d levels provides the energies for Pr^{3+} or Tb^{3+}; see figures 3 and 4. $\mathrm{Sh_d}$ is for each lanthanide a different constant that does not depend on the type of compound. By introducing a set of $\mathrm{Sh_f}$ energy shift operations, the levels belonging to states with excited $4f^{n-1}$ cores can be generated. The effect of the isotropic exchange interaction between the 5d electron spin and total spin of the $4f^{n-1}$ electrons can be accounted for by a third shift operation ($\mathrm{Sh_{ex}}$).

The so-called shift model is a crude model with limitations. It does not account for the $H^{\mathrm{so}}_{\mathrm{f}}$ interaction—see equation (8)—responsible for additional structure in the Pr^{3+} 4f5d level scheme. The situation is much more favourable for Tb^{3+}. Because the 5d spin–orbit interaction is quenched in compounds and because $L_{\mathrm{f}} = 0$ for Tb^{3+}, in theory the interaction $H^{\mathrm{so}}_{\mathrm{f}} = 0$. Furthermore, the $4f^7[^6\mathrm{P}]5d_1[\mathrm{HS}]$ state is always higher than the $4f^7[^7\mathrm{S}]5d_5[\mathrm{LS}]$ state. Because of this, the shift model applies particularly well for Tb^{3+}. This makes Tb^{3+} ideally suited for testing to what extent V_{d} is a lanthanide invariant and $H^{\mathrm{ex}}_{\mathrm{fd}}$ a compound invariant interaction.

The following conclusions were drawn:

(1) The 10 pm smaller size of Tb^{3+} as compared to Ce^{3+} results in different crystal field splittings. They tend to be smaller for Tb^{3+} when a small site is occupied. When large sites are occupied, a lattice relaxation may result in an enhanced splitting. The lanthanide contraction and its effect on crystal field splitting are regarded as the main contributions to the dispersion in the red-shift values $D(n, Q, \mathrm{A})$ with n; see equation (1) and figure 6.
(2) The exchange splitting between [HS] and [LS] states is in a first approximation the same for each $5d_i$ state.
(3) The size of the exchange splitting decreases with increasing covalency between 5d orbital and ligand orbitals. This results in an almost linear decrease with increasing centroid shift—see figure 8—or with increasing anion polarizability—see figure 9. At the same time, the oscillator strength of the spin forbidden transition to $5d_1$[HS] tends to increase;

see table 1. Both effects were explained by the decrease in the spin purity of the $5d_1$ state due to orbital mixing.

(4) The intensity of transitions to $5d_i$[HS] states increases with i. This is seen for $i = 1, 2, 3$ in figure 4.

(5) A splitting of $5d_i$[HS] in Tb^{3+} was never observed, indicating that the effect of H_f^{so} and H_d^{so} is negligible in compounds.

(6) The shift model applies particularly well for Tb^{3+}. It provides an easy method for assigning the bands observed.

References

[1] Dorenbos P 2003 *J. Phys.: Condens. Matter* **15** 575
[2] Dorenbos P 2000 *Phys. Rev.* B **62** 15640
[3] Bettinelli M and Mongorge R 2001 *J. Lumin.* **92** 287
[4] Dorenbos P 2002 *J. Alloys Compounds* **341** 156
[5] Ionova G, Krupa J C, Gerard I and Guillaumont R 1995 *New J. Chem.* **19** 677
[6] van Pieterson L, Reid M F, Wegh R T, Soverna S and Meijerink A 2002 *Phys. Rev.* B **65** 045113
[7] van Pieterson L, Reid M F, Burdick G W and Meijerink A 2002 *Phys. Rev.* B **65** 045114
[8] Reid M F, van Pieterson L and Meijerink A 2002 *J. Alloys Compounds* **344** 240
[9] Dorenbos P 2000 *J. Lumin.* **91** 155
[10] Dorenbos P 2000 *Phys. Rev.* B **62** 15650
[11] Dorenbos P 2001 *Phys. Rev.* B **64** 125117
[12] Dorenbos P 2002 *J. Lumin.* **99** 283
[13] Shannon R D 1976 *Acta Crystallogr.* A **32** 751
[14] Shi J and Zhang S 2003 *J. Phys.: Condens. Matter* **15** 4101
[15] Yanase A and Kasuya T 1970 *Suppl. Prog. Theor. Phys.* **46** 388
[16] Yanase A 1977 *J. Phys. Soc. Japan* **42** 1680
[17] Duan C K and Reid M F 2003 *J. Solid State Chem.* **171** 299
[18] Callahan W R 1963 *J. Opt. Soc. Am.* **53** 695
[19] Spector N and Sugar J 1976 *J. Opt. Soc. Am.* **66** 436
[20] Bryant B W 1965 *J. Opt. Soc. Am.* **55** 771
[21] Bland S W and Smith M J A 1985 *J. Phys. C: Solid State Phys.* **18** 1525
[22] Le Masson N L M, Vink A P, Dorenbos P, Bos A J J, van Eijk C W E and Chaminade J P 2003 *J. Lumin.* **101** 175
[23] Dieke G H and Crosswhite H M 1963 *Appl. Opt.* **2** 675
[24] Nakazawa E and Shiga F 2003 *Japan. J. Appl. Phys.* **42** 1642
[25] van der Kolk E, Dorenbos P, Vink A P, Perego R C, van Eijk C W E and Lakshmanan A R 2001 *Phys. Rev.* B **64** 195129
[26] van Pieterson L, Reid M F and Meijerink A 2002 *Phys. Rev. Lett.* **88** 067405
[27] Ranfagni A, Mugnai D, Bacci M, Viliani G and Fontana M P 1983 *Adv. Phys.* **32** 823
[28] Dorenbos P 2000 *J. Lumin.* **91** 91
[29] Popma Th J A, van der Weg W F and Thimm K 1981 *J. Lumin.* **24/25** 89
[30] Krupa J C, Mayolet A and Queffelec M 1998 *Ann. Chim. Sci. Mater.* **23** 431
[31] Saubat B, Fouassier C, Hagenmuller P and Bourcet J C 1981 *Mater. Res. Bull.* **15** 193
[32] Dorenbos P 2002 *Phys. Rev.* B **65** 235110
[33] Allred A L 1961 *J. Inorg. Nucl. Chem.* **17** 215
[34] Jörgensen C K 1971 *Modern Aspects of Ligand Field Theory* (Amsterdam: North-Holland)
[35] Dorenbos P, Andriessen J and van Eijk C W E 2003 *J. Solid State Chem.* **171** 133
[36] Meijerink A and Wegh R T 1999 *Mater. Sci. Forum* **315–317** 11
[37] Schlesinger M, Szczurek T and Wiltshire M C K 1976 *Can. J. Phys.* **54** 753
[38] Loh E 1968 *Phys. Rev.* **175** 533
[39] Wegh R T and Meijerink A 1999 *Phys. Rev.* B **60** 10820
[40] Krupa J C and Queffelec M 1997 *J. Alloys Compounds* **250** 287
[41] Ryan J L and Jörgensen C K 1966 *J. Phys. Chem.* **70** 2845
[42] Nugent L J, Baybarz R D, Burnett J L and Ryan J L 1973 *J. Phys. Chem.* **77** 1528
[43] Lammers M J J and Blasse G 1985 *Phys. Status Solidi* b **127** 663

[44] Blasse G and Bril A 1967 *Philips Res. Rep.* **22** 481
[45] You H, Wu X, Cui H and Hong G 2003 *J. Lumin.* **104** 223
[46] Brixner L H, Ackerman J F and Foris C M 1981 *J. Lumin.* **26** 1
[47] Hölsä J and Leskelä M 1981 *Phys. Status Solidi* b **103** 797
[48] Hölsä J 1980 *Finn. Chem. Lett.* 201
[49] Herzog G, Starick D, Birman T A, Golovkova S I and Gurvich A M 1992 *Phys. Status Solidi* a **130** K107
[50] Golovkova S I, Gurvich A M, Savikhina T I, Starick D, Birman T A, Herzog G, Katomina R V and Kra G 1981 *Zh. Prikl. Spektrosk.* **35** 806
[51] Li Y, Lu H, Li J and Miao X 1986 *J. Lumin.* **35** 107
[52] Yamashita N, Hamada T, Takada M, Katsuki M and Nakagawa M 2001 *Japan. J. Appl. Phys.* **40** 6732
[53] Blasse G and Bril A 1968 *Philips Res. Rep.* **23** 461
[54] Lenth W 1979 Übergangswahrscheinlichkeiten und Interionische Wechselwirkungen in Lasermaterialen aus reinen Seltenen Erd-Verbindungen *Thesis* University of Hamburg, Germany
[55] Kim C-H, Kwon I-E, Park C-H, Hwang Y-J, Bae H-S, Yu B-Y, Pyun C-H and Hong G-Y 2000 *J. Alloys Compounds* **311** 33
[56] Mayolet A 1995 Etude des processus d'absorption et de transfert d'energie au sein de materiaux inorganiques luminescents dans le domaine UV et VUV *Thesis* Université de Paris, XI Orsay
[57] Hoffman M V 1971 *J. Electrochem. Soc.: Solid State Sci.* **118** 1508
[58] Srivastava A M, Sobieraj M T, Valossis A, Ruan S K and Banks E 1990 *J. Electrochem. Soc.* **137** 2959
[59] Finke B, Schwarz L, Gürtler P and Kraas M 1992 *Phys. Status Solidi* a **130** K125
[60] Lee S and Seo S Y 2002 *J. Electrochem. Soc.* **149** J85
[61] Ropp R C and Carroll B 1977 *J. Phys. Chem.* **81** 746
[62] Finke B, Schwarz L, Gürtler P, Kraas M, Joppien M and Becker J 1994 *J. Lumin.* **60/61** 975
[63] Fava J, Perrin A, Bourcet J C, Salmon R, Parent C and Le Flem G 1979 *J. Lumin.* **18/19** 389
[64] Hoshina T and Kuboniwa S 1971 *J. Phys. Soc. Japan* **31** 828
[65] Brücher E and Zékány L 1981 *J. Inorg. Nucl. Chem.* **43** 351
[66] Svetashev A G and Tsvirko M P 1981 *Opt. Spectrosk.* **51** 572
[67] Carnall W T, Fields P R and Rajnak K 1968 *J. Chem. Phys.* **49** 4447
[68] You H, Wu X, Zeng X, Hong G, Kim C-H, Pyun C-H and Park C-H 2001 *Mater. Sci. Eng.* B **86** 11
[69] Tian F W, Fouassier C and Hagenmuller P 1987 *Mater. Res. Bull.* **22** 389
[70] Mayolet A, Zhang W, Martin P, Chassigneux B and Krupa J C 1996 *J. Electrochem. Soc.* **143** 330
[71] van der Voort D, de Rijk J M E, van Doorn R and Blasse G 1992 *Mater. Chem. Phys.* **31** 333
[72] Wanmaker W L and Bril A 1964 *Philips Res. Rep.* **199** 479
[73] You H, Hong G, Zeng X, Kim C-H, Pyun C-H, Yu B-Y and Bae H-S 2000 *J. Phys. Chem. Solids* **61** 1985
[74] Kellendonk F and Blasse G 1982 *J. Phys. Chem. Solids* **43** 481
[75] Blasse G and Bril A 1967 *Phys. Lett.* A **25** 29
[76] Veenis A W and Bril A 1978 *Philips J. Res.* **33** 124
[77] Hoshina T 1969 *J. Chem. Phys.* **50** 5258
[78] Koike J, Kojima T, Toyonaga R, Kagami A, Hase T and Inaho S 1979 *J. Electrochem. Soc.: Solid State Sci. Technol.* **126** 1008
[79] Rambabu U, Annapurna K, Balaji T, Satyanarayana J V, Rajamohan Reddy K and Buddhudu S 1996 *Spectrosc. Lett.* **29** 833
[80] Kwon I-E, Yu B-Y, Bae H, Hwang Y-J, Kwon I-W, Kim C-H, Pyun C H and Kim S-J 2000 *J. Lumin.* **87–89** 1039
[81] Hoshina T and Kuboniwa S 1972 *J. Phys. Soc. Japan* **32** 771
[82] Meiss D, Wischert W and Kemmler-Sack S 1992 *Phys. Status Solidi* a **134** 539
[83] Mayolet A and Krupa J C 1996 *J. Soc. Inform. Disp.* **4/3** 173
[84] McAllister W A 1966 *J. Electrochem. Soc.* **113** 226
[85] Wiehl J and Kemmler-Sack S 1990 *Z. Naturf.* a **45** 1293
[86] Lammers M J J and Blasse G 1987 *J. Electrochem. Soc.: Solid State Sci. Technol.* **134** 2068
[87] Choi Y Y, Sohn K-S, Park H D and Choi S Y 2001 *J. Mater. Res.* **16** 881
[88] Lin J, Su Q, Zhang H and Wang S 1996 *Mater. Res. Bull.* **31** 189
[89] Reichardt J, Stiebler M, Hirrle R and Kemmler-Sack S 1990 *Phys. Status Solidi* a **119** 631
[90] Meiss D, Wischert W and Kemmler-Sack S 1994 *Mater. Chem. Phys.* **38** 191
[91] Lin J and Su Q 1995 *J. Mater. Chem.* **5** 1151
[92] Jia D, Meltzer R S, Yen W M, Jia W and Wang X 2002 *Appl. Phys. Lett.* **80** 1535
[93] Jia D, Wang X-J and Yen W M 2002 *Chem. Phys. Lett.* **363** 241
[94] Kubota S, Isumi M, Yamane H and Shimada M 1999 *J. Alloys Compounds* **283** 95

[95] Fava J, Le Flem G, Bourcet J C and Gaume-Mahn F 1976 *Mater. Res. Bull.* **11** 1
[96] de Vries A J and Blasse G 1987 *Mater. Res. Bull.* **22** 1141
[97] Lammers M J J, Severin J W and Blasse G 1987 *J. Electrochem. Soc.: Solid State Sci. Technol.* **134** 2356
[98] Mayolet A, Zhang W, Simoni E, Krupa J C and Martin P 1995 *Opt. Mater.* **4** 757
[99] Choe J Y, Ravichandran D, Blomquist S M, Kirchner K W, Forsythe E W and Morton D C 2001 *J. Lumin.* **93** 119
[100] Liu X, Wang X, Ma L, Shen W and Wang Z 1988 *J. Lumin.* **40/41** 653
[101] Brixner L H 1984 *Mater. Res. Bull.* **19** 143
[102] Blasse G and Dirksen G J 1989 *J. Electrochem. Soc.* **136** 1550
[103] Kubota S, Suzuyama Y, Yamane H and Shimada M 1998 *J. Alloys Compounds* **268** 66
[104] Zych E 2001 *Opt. Mater.* **16** 445